



HAL
open science

A new pharmacokinetic model for ^{90}Y -ibritumomab tiuxetan based on 3-dimensional dosimetry

Franck Morschhauser, Berengere Dekyndt, Clio Baillet, Christine Barthelemy, E Malek, J Fulcrand, P Bigot, Damien Huglo, Bertrand Decaudin, Nicolas Simon, et al.

► To cite this version:

Franck Morschhauser, Berengere Dekyndt, Clio Baillet, Christine Barthelemy, E Malek, et al.. A new pharmacokinetic model for ^{90}Y -ibritumomab tiuxetan based on 3-dimensional dosimetry. Scientific Reports, 2018, Scientific Reports, 8, pp.14860. 10.1038/s41598-018-33160-0 . hal-02148590

HAL Id: hal-02148590

<https://hal.univ-lille.fr/hal-02148590>

Submitted on 7 Jun 2021

HAL is a multi-disciplinary open access archive for the deposit and dissemination of scientific research documents, whether they are published or not. The documents may come from teaching and research institutions in France or abroad, or from public or private research centers.

L'archive ouverte pluridisciplinaire **HAL**, est destinée au dépôt et à la diffusion de documents scientifiques de niveau recherche, publiés ou non, émanant des établissements d'enseignement et de recherche français ou étrangers, des laboratoires publics ou privés.



Distributed under a Creative Commons Attribution 4.0 International License

SCIENTIFIC REPORTS



OPEN

A new pharmacokinetic model for ^{90}Y -ibritumomab tiuxetan based on 3-dimensional dosimetry

F. Morschhauser^{1,2}, B. Dekyndt^{1,3}, C. Baillet^{1,4}, C. Barthélémy¹, E. Malek¹, J. Fulcrand¹, P. Bigot¹, D. Huglo⁴, B. Décaudin^{1,3}, N. Simon^{1,3}  & P. Odou^{1,3}

Monoclonal antibodies (mAbs) are key components in several therapies for cancer and inflammatory diseases but current knowledge of their clinical pharmacokinetics and distribution in human tissues remains incomplete. Consequently, optimal dosing and scheduling in clinics are affected. With sequential radiolabeled mAb-based imaging, radiation dosing in tissues/organs can be calculated to provide a better assessment of mAb concentrations in tissues. This is the first pharmacokinetic model of ^{90}Y -Ibritumomab tiuxetan (^{90}Y -IT) in humans to be described, based on three-dimensional (3D) dosimetry using single-photon emission computed-tomography coupled with computed-tomography. 19 patients with follicular lymphoma were treated initially with ^{90}Y -IT in the FIZZ trial. Based on a compartmental approach individualising the vascular compartment within studied organs, this study proposes a reliable pharmacokinetic (PK) five-compartment model replacing the currently used two-compartment model and constitutes a new direction for further research. This model provides exchange constants between the different tissues, Area Under the Curve of ^{111}In -IT in blood (AUC) and Mean Residence Time (MRT) that have not been reported so far for IT. Finally, the elimination process appears to occur in a compartment other than the liver or the spleen and suggests the metabolism of mAbs may take place mainly on the vascular compartment level.

Monoclonal antibodies (mAbs) whether alone or coupled with radioisotopes or cytotoxic drugs^{1,2} are key components in therapies for many cancers and inflammatory diseases. In spite of their widespread clinical use, literature on mAb clinical pharmacokinetics (PK) remains sparse and little is known about mAb distribution in tissues³⁻⁵, which considerably complicates the defining of optimal mAb dosing and scheduling in clinical practice. Non-compartmental analysis, the most common approach to analysing PK data in drug development, requires a large amount of data and samples per individual to obtain precise PK parameter estimations and is inadequate for studying mAb behaviour⁶. With compartmental analysis, The mAb standard PK model is a two compartment model (central and peripheral), which can assess mAb kinetics in blood but not their distribution in tissues. Fronton *et al.*⁷ showed that this model is not compliant with current knowledge. Sequential imaging of radiolabeled mAbs *in vivo* means that the absorbed radiation dose as well as mAb concentrations can be calculated⁸⁻¹¹. Radioimmunotherapy (RIT) - a targeted therapy using monoclonal antibodies (mAbs) directed to tumor-associated antigens to deliver irradiation from radionuclides to the tumor - is therefore a particularly attractive tool to modelise mAb PK in patients. For many years, two-dimensional (2D) imaging (planar whole-body scintigraphy (anterior and posterior views))¹² has been the method of choice for dosimetric studies in RIT despite significant uncertainties in organ volume measurements affecting the accuracy of dosimetric estimates. Nowadays, it is possible to obtain more accurate radiation dose estimation in tissues/organs with three-dimensional (3D) dosimetry using single-photon emission computed-tomography coupled with computed-tomography (SPECT-CT)¹³⁻¹⁶, or Positron Emission Tomography coupled with computed-tomography (PET-CT)^{17,18}.

¹Univ. Lille, CHU Lille, EA 7365 – GRITA – Groupe de Recherche sur les formes Injectables et les Technologies Associees, Lille, France. ²Haematology Department, Hôpital Claude Huriez, CHU Lille, F-59000, Lille, France. ³Pharmacy Institute, CHU Lille, F-59000, Lille, France. ⁴Nuclear Medicine department, Hôpital Claude Huriez, CHU Lille, F-59000, Lille, France. Correspondence and requests for materials should be addressed to F.M. (email: franck.morschhauser@chru-lille.fr)

	F1	F2	p
Patients	19	13	/
Gender ratio (M/F)	5/14	3/10	0.885
Age* (years)	58.8 (28–80)	59.6 (28–80)	0.954
Weight* (kg)	71.2 (49–100)	72.9 (49–83)	0.744
Height* (cm)	165.2 (157–185)	164.8 (157–185)	0.832
Body mass index* (kg.m ⁻²)	26.0 (17.6–32.5)	26.8 (17.6–32.5)	0.658
Body Surface Area* (m ²)	1.82 (1.49–2.28)	1.83 (1.51–2.28)	0.803
Tumor volume* (mm ³)	6751 (150–25855)	1850 (0–8859)	0.001
FLIPI Score	Low Risk	6	0.907
	Intermediate Risk	4	
	High Risk	9	

Table 1. Patient characteristics at baseline. *Mean (range).

Area	Lumbar vertebrae L2-L4	Liver	Spleen
Blood in corresponding volume* (mL)	8.15 (2.81)	485 (174)	81.5 (53.7)
Blood in mL.g ⁻¹ of organ*	0.15 (0.03)	0.29 (0.05)	0.28 (0.04)

Table 2. Volume of blood estimated in each organ. *Mean (Standard deviation).

Accurate mAb PK modeling requires individualised estimations of antibody concentrations in the vascular compartment within each organ. This individualising appears feasible with dosimetric studies¹⁹ but has not been applied in 3D dosimetric studies so far.

Yttrium 90 - Ibritumomab tiuxetan (Y90-IT) is a drug consisting of a murine anti-CD20 antibody (ibritumomab) linked to a chelator (tiuxetan) radiolabeled with 90-Yttrium (YTRACIS, Curium Pharma) according to the method described in the Zevalin monograph (ZEVALIN, Spectrum Pharmaceuticals BV) for therapy or 111-Indium for imaging (Indium 111 Chlorure, Curium Pharma) according to the method described by Ferrer *et al.*²⁰. It has been approved for the treatment of follicular lymphoma (FL) in case of relapse or refractory disease or to consolidate first-line therapy. The recently reported FIZZ Study showed that fractionated RIT is effective as initial treatment for advanced-stage FL in patients with a high tumor burden²¹. Following the protocol, a subset of FIZZ patients underwent a patient-specific 3D dosimetric study.

This is the first description of a pharmacokinetic model of ⁹⁰Y-Ibritumomab tiuxetan in humans, based on dosimetric and 3D-imaging data obtained from FIZZ patients, coupled with a pharmacokinetic compartmental approach and individualising the vascular compartment within the organs studied. This method allows describing all compartments in which mAb was measured.

Results

Patients. 3D imaging data after the first fraction (F1) of RIT was available for 19 patients and after the 2 fractions (F1 and F2) for 13 patients since the second fraction was cancelled for 6 patients due to hematologic toxicity after F1 or the development of HAMA. Baseline characteristics are listed in Table 1. Only tumor volume is significantly different between F1 and F2 (6751 and 1850 mm³ respectively).

Concentration-time profiles. Estimated blood volumes of lumbar vertebrae L2-L4 (8.15 mL), liver (485 mL) and spleen (81.5 mL) are shown in Table 2.

The calculation method for mAb amount in blood vessels within organs and tissues is shown in Fig. 1. Radiolabeled mAb concentrations in blood and organs (concentration-time profiles) are reported in Fig. 2.

Pharmacokinetic model. The model selected with Kinetica[®] software to best predict the biodistribution of Ibritumomab tiuxetan is shown in Fig. 3. This model is a 5-compartment model (including blood, bone-vertebrae L2-L4, liver, spleen plus a deep compartment). In this model, ibritumomab tiuxetan is infused into blood. The vascular compartment is considered as the central compartment, from which mAbs diffuse in both directions to other compartments, except for the spleen. Radiolabeled mAbs diffuse into the spleen from the blood and are cleared by the liver. The pharmacokinetic constants are order one constants. The deep compartment (number 5) includes the remaining organs and the tumor.

Pharmacokinetic parameters. The pharmacokinetic parameters for the various compartments (blood, L2-L4 vertebrae, liver and spleen) from Kinetica[®] software are reported in Table 3. Some parameters are significantly different from F1 to F2, especially for the vertebrae L1-L2 (the distribution constant k_{12} and the AUCcum 7d* (µg.min.mL⁻¹) are higher for F1 than F2) and Spleen compartments (the Cmax, the distribution constant, the AUCcum 4d and AUCcum 7d are higher for F1 than F2 and the elimination constant is lower for F1 than F2).

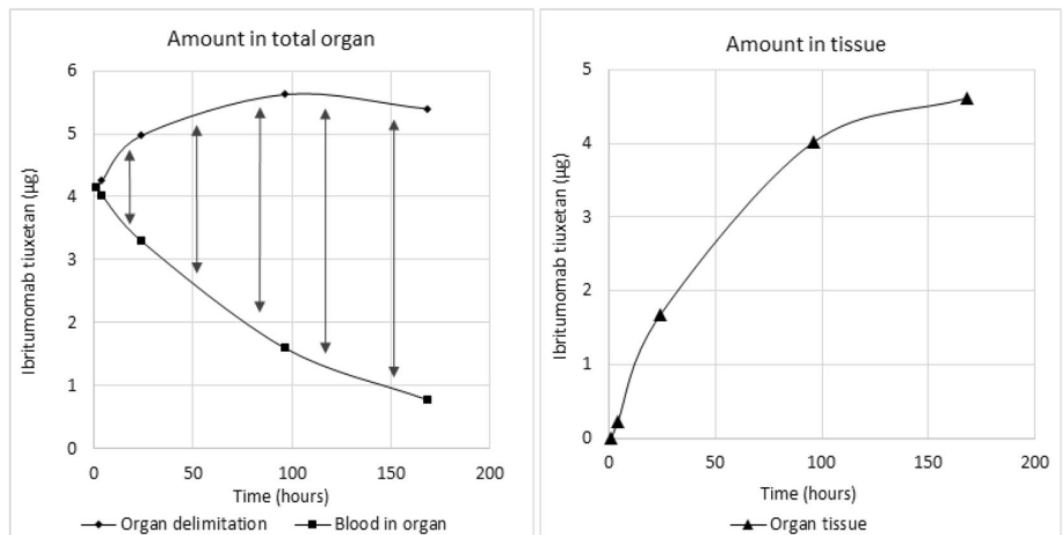


Figure 1. Subtraction of the blood constituent of Ibritumomab tiuxetan from total organ to obtain the remaining tissue constituent

Discussion

Among the thirty pharmacokinetic models assessed, the best pharmacokinetic model according to the AKAIKE test, validated on both RIT fractions, is a five-compartment model close to a mammalian PK model, except for the spleen. It provides exchange constants between the different tissues, AUC and MRT that have not yet been reported for Ibritumomab tiuxetan. Very little data is available on the elimination pathways of therapeutic mAbs. In our model, which individualises the vascular compartment within organs, the elimination process appears to be performed by a compartment other than that of the liver or the spleen and suggests the metabolism of mAbs may take place mainly on the vascular compartment level. This finding is in keeping with published data suggesting that monoclonal antibodies may be metabolised in the vascular compartment by endothelial cells and, to a much lesser extent (5.9%) urinary excretion^{22–27}. Other studies, investigating the exact amount of urinary excretion through urinary sampling could provide further details on elimination pathways. However, biliary and renal excretions are known to be minimal^{22–25}.

The pharmacokinetic parameters of the model concord with data in literature, thereby confirming its reliability. The mean blood half-life of ¹¹¹In-ibritumomab tiuxetan is 83.6 and 83.8 hours for F1 and F2, respectively and varies between 20 and 140 hours in the literature^{24,28}. The volume of blood in the liver (489.61 mL and 459.72 mL for F1 and F2 respectively) and in the spleen (81.22 mL and 65.28 mL) are in keeping with previously published estimates²⁵. The Volumes of distribution (Vd) estimated by our model are 4131.0 and 4064.3 mL for F1 and F2, respectively. These figures are slightly lower than published data (5000–10000 mL²⁹). Nevertheless the calculated volumes of distribution (our results and published data) remain small, suggesting a limited distribution outside the blood^{29,30} (29,30)(28,29). These results can be accounted for by mAb properties such as high molecular mass and hydrophilicity/polarity ratio. Other parameters cannot be compared with scientific literature as they are rarely described.

Although our 5-compartment model is a step forward compared to the previous 2-compartment model, there are clear limitations. First, in dosimetric studies, the data used to delineate organs is usually obtained with few samples: three^{31,32}, four³⁰, five^{24,33,34} or even fewer³⁵ but this reduced sampling can prove limiting for pharmacokinetic studies. The number of image acquisitions was four (4 hours, 1, 4 and 7 days after infusions) The extrapolation method to determine the amount of blood in organs would have been more precise if imaging had been performed 1 hour after infusion, instead of 4 hours but this is problematic given the possible occurrence of infusion-related reactions to mAb. Also, the dosimetric study was limited to 7 days (taking into account the radioactive period of Indium 111 which is 67 hours). The presence of residual radioactivity prevented a precise calculation of the elimination constants since the completed diffusion phase could not be assessed. It has to be acknowledged that 4 samples is already considerable as a whole body SPECT/CT examination is a time/device-consuming procedure (about 1 hour per image) and an inconvenience to patients.

A second limitation is that the compartment representing the tumor was not individualised. Tumor volume was significantly lower before F2 than F1 (1850 and 6751 mm³ respectively), as a consequence of tumor reduction after the first RIT fraction³⁶. It should be noted that mAb concentrations were higher in blood and liver and lower in the spleen and lumbar vertebrae at F2 with significant changes in the PK parameters of “L2-L4 vertebrae” and “spleen”. This may be explained by tumor regression during the time between F1 and F2 which would modify the fifth compartment. Another study has revealed baseline metabolic tumor volume influence on mAb exposure³⁷. Evaluating radiolabeled mAb distribution in the tumor compartment is difficult and tedious, in particular for small tumors. PET imaging would yield more precise quantifications due to its better spatial resolution than SPECT and to its more elaborate quantification tools. Major progress has been made in immunoPET since this

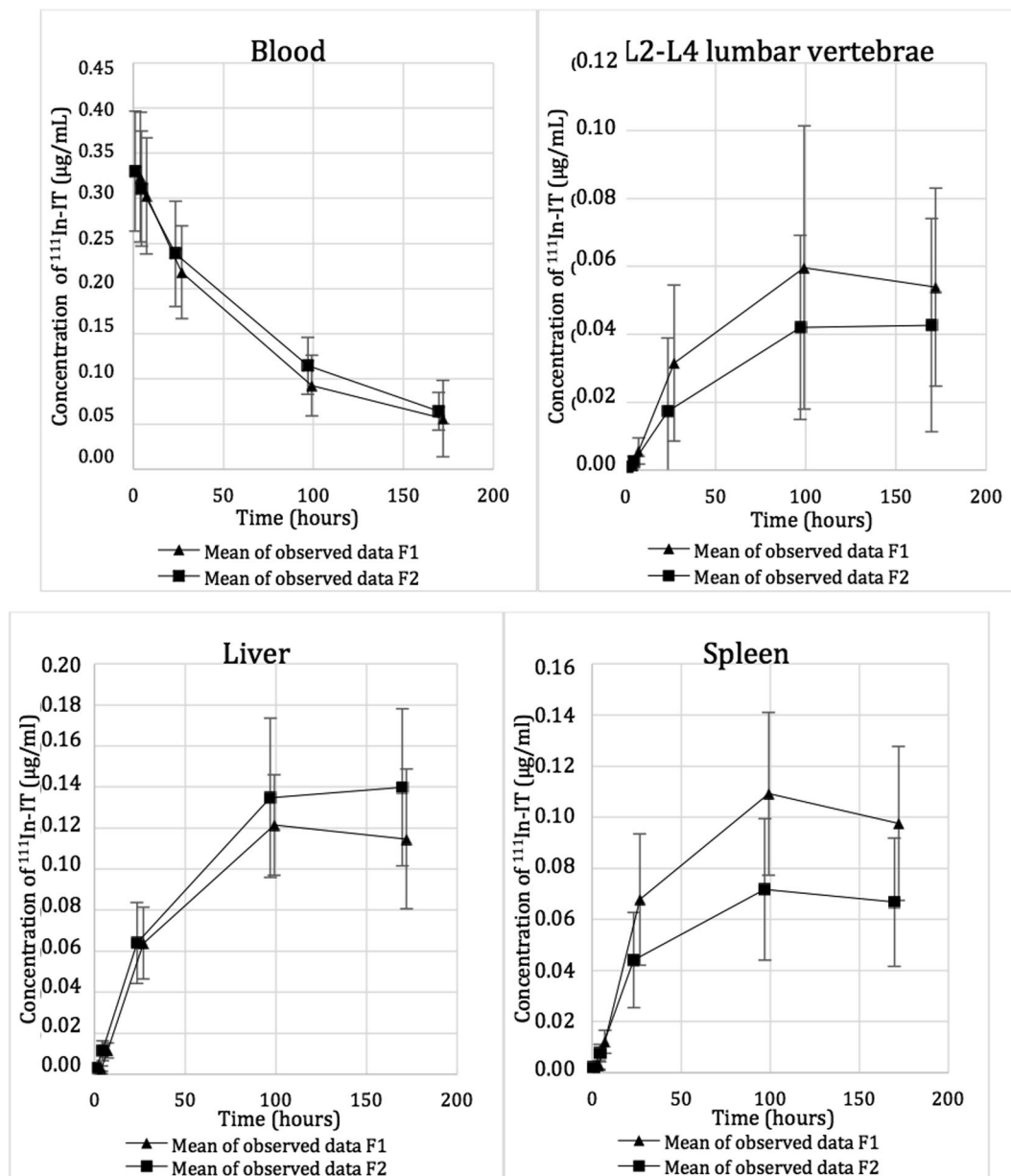


Figure 2. Evolution of $^{111}\text{In-IT}$ concentration in blood and organ tissues.

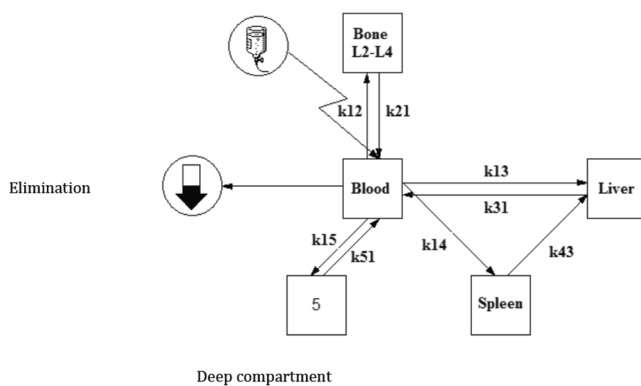


Figure 3. Model selected for best biodistribution fit.

		F1	F2	p
Blood	Vd* (mL)	4131.0 (937.1)	4064.8 (970.1)	0.568
	Cmax* ($\mu\text{g}\cdot\text{mL}^{-1}$)	0.308 (0.086)	0.326 (0.064)	0.539
	T1/2* (h)	83.6 (37.5)	83.8 (13.5)	0.34
	MRT* (h)	114.1 (57.0)	116.0 (17.0)	0.250
	Clearance* (mL.min)	1.03 (0.73)	0.74 (0.25)	0.179
	AUC Total* ($\mu\text{g}\cdot\text{min}\cdot\text{mL}^{-1}$)	1708.1 (820.0)	1983.7 (588.7)	0.179
Vertebrae L2-L4	Volume of blood* (mL)	7.84 (2.44)	7.87 (2.21)	0.944
	Cmax* ($\mu\text{g}\cdot\text{mL}^{-1}$)	0.071 (0.066)	0.046 (0.032)	0.099
	k_{12} * (min^{-1})	1.11 E-4 (1.31 E-4)	0.60 E-4 (0.55 E-4)	0.033
	k_{21} * (min^{-1})	1.05 E-4 (0.55 E-4)	0.96 E-4 (0.57 E-4)	0.516
	MRT* (h)	424.8 (136.5)	519.3 (227.2)	0.296
	AUCcum 4d* ($\mu\text{g}\cdot\text{min}\cdot\text{mL}^{-1}$)	261.98 (251.16)	145.11 (113.73)	0.054
	AUCcum 7d* ($\mu\text{g}\cdot\text{min}\cdot\text{mL}^{-1}$)	558.03 (530.77)	329.24 (249.35)	0.039
Liver	Volume of blood* (mL)	489.61 (178.26)	459.72 (149.07)	0.558
	Cmax* ($\mu\text{g}\cdot\text{mL}^{-1}$)	0.182 (0.126)	0.359 (0.159)	0.103
	k_{13} * (min^{-1})	1.80 E-4 (0.60 E-4)	2.05 E-4 (1.70 E-4)	0.738
	k_{31} * (min^{-1})	2.32 E-4 (1.07 E-4)	1.77 E-4 (0.25 E-4)	0.167
	MRT* (h)	381.4 (99.9)	419.6 (120.1)	0.357
	AUCcum 4d* ($\mu\text{g}\cdot\text{min}\cdot\text{mL}^{-1}$)	449.72 (99.34)	548.59 (270.41)	0.277
	AUCcum 7d* ($\mu\text{g}\cdot\text{min}\cdot\text{mL}^{-1}$)	979.63 (216.09)	1220.50 (583.78)	0.132
Spleen	Volume of blood* (mL)	81.22 (55.34)	65.28 (45.96)	0.295
	Cmax* ($\mu\text{g}\cdot\text{mL}^{-1}$)	0.125 (0.059)	0.073 (0.027)	0.001
	k_{13} * (min^{-1})	2.11 E-4 (1.39 E-4)	1.17 E-4 (0.52 E-4)	0.005
	k_{31} * (min^{-1})	1.26 E-4 (0.50 E-4)	1.64 E-4 (0.40 E-4)	0.045
	MRT* (h)	375.9 (119.1)	392.3 (125.5)	0.802
	AUCcum 4d* ($\mu\text{g}\cdot\text{min}\cdot\text{mL}^{-1}$)	471.81 (230.56)	286.67 (113.86)	0.008
	AUCcum 7d* ($\mu\text{g}\cdot\text{min}\cdot\text{mL}^{-1}$)	980.15 (465.22)	588.20 (225.95)	0.004

Table 3. Comparison of PK parameters in F1 and F2. *Mean (Standard Deviation).

study was first designed with the development of Zr89 labelled mAbs resulting in PET biodistribution studies^{38,39}. It should therefore be easier to estimate the volume of tumoral lesions and, their evolution as well as modifications in radiolabeled mAb kinetics from one fraction to the other. A study has shown that CD20 expression can be induced by low dose gamma-radiation which could account for the difference in antibody distribution between the F1 and F2 fractions⁴⁰. Another explanation could be metabolism by the internalising⁴¹ of surface CD20 receptors following their association with an anti-CD20 antibody or CD20 modulation⁴².

The PK parameters described in this study are numerous and relevant and constitute a background for further research. The study proposes a reliable pharmacokinetic five-compartment model of ⁹⁰Y-Ibritumomab tiuxetan. The main limitation to the model concerns the tumor compartment, which is not separated from the rest of the tissues. Differences in dosimetry and pharmacokinetic parameters (radiolabeled mAb concentrations, diffusion and elimination) for certain tissues might be better clarified with further investigations based on immunoPET and broader biological sampling.

Material and Methods

Patients. Patients with histologically confirmed CD20-positive Follicular Lymphoma were included in the FIZZ study (NCT01493479 and Northwest Ethical Research Committee IV)³⁶.

The FIZZ study was a multi-centre, non-randomised prospective phase II study of fractionated ⁹⁰Y-Ibritumomab tiuxetan as the initial therapy for follicular lymphoma (FL) in patients in need of treatment according to GELF/BNLI criteria. Briefly, treatment consisted of 2 infusions, termed fraction 1 (F1) and 2 (F2) of ⁹⁰Y-ibritumomab tiuxetan (11.1 MBq/kg per fraction; maximal dose 888 MBq) given 8–12 weeks apart (Fig. 4) provided the platelet count was $>150 \times 10^9/\text{L}$ (2nd infusion) and neutrophil count $>1.5 \times 10^9/\text{L}$. Occurrence of grade 3 or grade 4 myelotoxicity after 2 weeks, or a Human anti-mouse antibody (HAMA) reaction led to exclusion from a second ⁹⁰Y-ibritumomab tiuxetan infusion. Patients with $>20\%$ lymphoma infiltration of bone marrow (BM) received 4 weekly infusions of Rituximab (375 mg/m²) (RTX) and proceeded to fractionated RIT only if a repeat BM biopsy demonstrated clearing of lymphoma to $<20\%$ involvement. Each ⁹⁰Y-ibritumomab tiuxetan fraction was preceded by two rituximab infusions (250 mg/m²) given 7–8 days apart, the second infusion given immediately prior to ⁹⁰Y-ibritumomab tiuxetan in order to saturate the binding sites of circulating anti-CD20 antibodies.

Dosimetric study. Raw data used to establish a pharmacokinetic model of ⁹⁰Y-Ibritumomab tiuxetan (IT) was obtained from the patients included in the FIZZ trial at Lille university hospital.

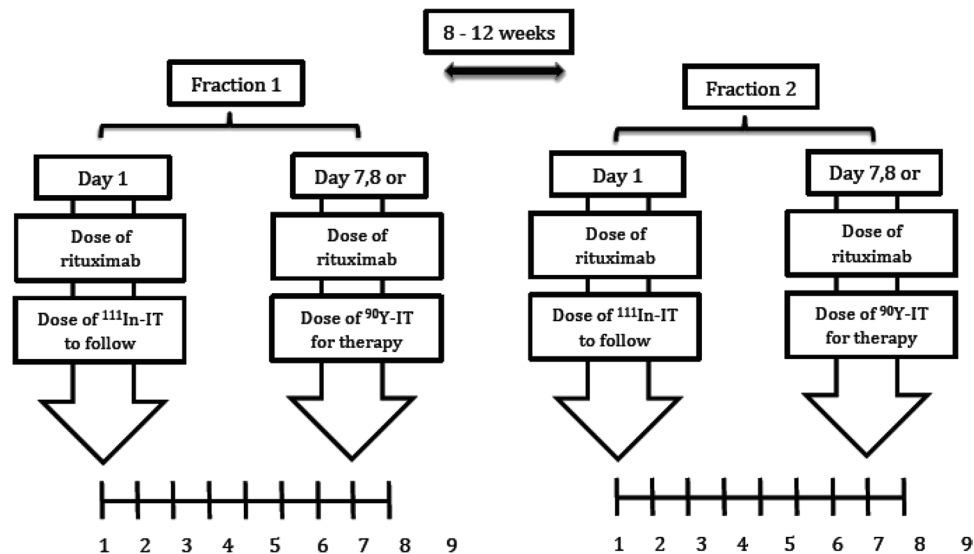


Figure 4. FIZZ trial design.

Following protocol, a subset of FIZZ patients underwent a patient-specific 3D dosimetric study with 138 MBq of ¹¹¹In-ibritumomab tiuxetan (¹¹¹In-ibritumomab tiuxetan administered intravenously concomitantly with the first rituximab infusion) for both ⁹⁰Y-ibritumomab tiuxetan fractions²¹.

Radiolabeling. Radiolabeling was performed with 222 MBq of ¹¹¹In for 1.6 mg ibritumomab tiuxetan (specific activity of 138 MBq/mg). The radiochemical purity threshold for injection to the patient was set at 95%.

Imaging method. Whole body Single-photon emission computed-tomography (SPECT)/Computed-Tomography (CT) (MEAP colimators, Siemens medical solution, Symbia T2, Erlangen, Germany) was performed at 4 hours, 24 h, 96 h and 168 h after infusions. A CT scan was performed to delineate the organs of interest (liver, spleen, bone marrow) plus tumor volume. Concentration of radioactivity in each of these organs was determined on SPECT imaging by the count number in the respective volumes²¹. The absorbed bone marrow dose was assessed on the L2-L4 lumbar area according to Shen *et al.*⁴³.

The accurate processing of 3D images to confirm absorbed-dose calculations (using CT images to estimate patient-specific organ and bone marrow volumes) was centralised in the CRCNA laboratory (Nantes) as previously²¹. All patients provided informed written consent. Ethics approval was granted in accordance with French and UK Medical Research Council guidelines and the Declaration of Helsinki (NCT01493479). All methods were performed in accordance with the relevant guidelines and regulations.

Blood samples study. *Blood vessel compartment in each organ.* Antibody diffusion was assumed to consist of a vascular phase (from a few minutes until one hour after injection) and a tissue phase. After one hour, when antibody concentration in blood is maximal and before the tissue phase, the blood volume in each organ was extrapolated, by dividing the amount of ¹¹¹In-IT in the whole organ (whole body SPECT/CT performed 4 hours after injection) by the concentration of ¹¹¹In-IT in peripheral blood (sample taken 1 h after injection). Organ mass was determined using the CT scan.

Determination of amounts of radiolabeled mAbs in blood. The amount of radioelement in peripheral blood was calculated through decay correction and correspondence between mass and activity (activity concentration). Blood radioactivity was determined using a well counter (Packard Cobra Gamma counter, GMI Inc, Minnesota, USA) (efficiency = 93.3%). Radiolabeled antibodies were considered to be the only source of radioactivity in blood samples. The amount of ¹¹¹In-ibritumomab tiuxetan in blood was then calculated as follows.

$$Am_{ibr} = \frac{Ac/0.933}{e^{-\frac{\ln(2)}{T_{1/2}^{in}} \cdot t}} \times MAC$$

Where:

- Am_{ibr} is the amount of ¹¹¹In-Ibritumomab tiuxetan, expressed in milligrams in the blood sample.
- Ac is the detected radioactivity, expressed in MBq.
- $T_{1/2}^{in}$ is the radioactive half-life of ¹¹¹In.
- MAC is the activity concentration. Here, the value was 138 MBq/mg.

At each sampling time, amounts of radiolabeled mAbs in blood in organs were calculated as follows:

$$Am_{ibr \text{ Blood in organ}} = Am_{ibr} \times V_{\text{Blood in the organ}}$$

Determination of amounts of radiolabeled mAbs in tissues. The amount of mAbs in each tissue was determined by subtracting the amount of radiolabeled mAbs in blood from the total amount of radiolabeled mAbs in organs at each sampling time.

Pharmacokinetic model building and Modelling. The Designer module of Kinetica[®] software v5.0 (Thermo Fisher Scientific) was used to estimate the PK parameters of Ibritumomab tiuxetan from radiolabeled-mAb blood and organ concentrations. The quality of PK models was assessed by the Akaike Information Criterion (AIC). The best AIC score (43) indicated the most accurate model to describe PK data. The model was built from pharmacokinetic parameters which were evaluated for each patient.

These are expressed as

- $k_{x_1x_2}$ being the order one rate constant from the x_1 compartment to the x_2 compartment.
- x_1, x_2, x_3, x_4 and x_5 respectively represent blood, L2-L4 vertebrae, liver, spleen and a deep compartment, considered as the other compartments of the organism (including tumor volume).
- k_{el} is the elimination constant rate from the blood compartment (order one).
- V_d is the distribution volume (V_d).
- $T_{1/2}$ is the mAb biological half-life.
- CL_T is the total clearance.
- AUC is the total Area Under the Curve of ¹¹¹In-Ibritumomab tiuxetan in blood.

Organ blood volumes were measured. The cumulated AUC at four (AUCcum 4d) and seven (AUCcum 7d) days after injection of ¹¹¹In-Ibritumomab tiuxetan was calculated.

For each compartment, the Mean Residence Time (MRT) and maximal concentration (Cmax) of ¹¹¹In-Ibritumomab tiuxetan were calculated.

Statistical analysis. Data obtained after F1 and F2 was not pooled and the pharmacokinetic model was first established on data obtained after F1, followed by that obtained after F2. Parameters are expressed as mean values and standard deviation or mean values and range of variation. They were compared using the bilateral non-parametric Mann–Whitney test ($\alpha = 0.05$) with XLSTAT[®] software (version 2012.2.03, Addinsoft).

References

1. Kuroki, M. *et al.* Possible applications of antibodies or their genes in cancer therapy. *Anticancer Res.* **26**, 4019–4025 (2006).
2. Guillemard, V. & Saragovi, H. U. Novel approaches for targeted cancer therapy. *Curr. Cancer Drug Targets* **4**, 313–326 (2004).
3. Keizer, R. J., Huitema, A. D. R., Schellens, J. H. M. & Beijnen, J. H. Clinical pharmacokinetics of therapeutic monoclonal antibodies. *Clin. Pharmacokinet.* **49**, 493–507 (2010).
4. Paintaud, G. Pharmacokinetics (PK) of mAbs. *Med. Sci. MS* **25**, 1057–1062 (2009).
5. Dostalek, M., Gardner, I., Gurbaxani, B. M., Rose, R. H. & Chetty, M. Pharmacokinetics, pharmacodynamics and physiologically-based pharmacokinetic modelling of monoclonal antibodies. *Clin. Pharmacokinet.* **52**, 83–124 (2013).
6. Davda, J. P., Dodds, M. G., Gibbs, M. A., Wisdom, W. & Gibbs, J. A model-based meta-analysis of monoclonal antibody pharmacokinetics to guide optimal first-in-human study design. *mAbs* **6**, 1094–1102 (2014).
7. Fronton, L., Pilari, S. & Huisinga, W. Monoclonal antibody disposition: a simplified PBPK model and its implications for the derivation and interpretation of classical compartment models. *J. Pharmacokinet. Pharmacodyn.* **41**, 87–107 (2014).
8. Sepp, A., Berges, A., Sanderson, A. & Meno-Tetang, G. Development of a physiologically based pharmacokinetic model for a domain antibody in mice using the two-pore theory. *J. Pharmacokinet. Pharmacodyn.* **42**, 97–109 (2015).
9. Garg, A. & Balthasar, J. P. Physiologically-based pharmacokinetic (PBPK) model to predict IgG tissue kinetics in wild-type and FcRn-knockout mice. *J. Pharmacokinet. Pharmacodyn.* **34**, 687–709 (2007).
10. Kletting, P., Bunjes, D., Reske, S. N. & Glatting, G. Improving anti-CD45 antibody radioimmunotherapy using a physiologically based pharmacokinetic model. *J. Nucl. Med. Off. Publ. Soc. Nucl. Med.* **50**, 296–302 (2009).
11. Kletting, P. *et al.* Radioimmunotherapy with anti-CD66 antibody: improving the biodistribution using a physiologically based pharmacokinetic model. *J. Nucl. Med. Off. Publ. Soc. Nucl. Med.* **51**, 484–491 (2010).
12. Fleming, J. S. A technique for the absolute measurement of activity using a gamma camera and computer. *Phys. Med. Biol.* **24**, 176–180 (1979).
13. Da Silva, A. J. *et al.* Absolute quantification of regional myocardial uptake of ^{99m}Tc-sestamibi with SPECT: experimental validation in a porcine model. *J. Nucl. Med. Off. Publ. Soc. Nucl. Med.* **42**, 772–779 (2001).
14. Ritt, P., Vija, H., Hornegger, J. & Kuwert, T. Absolute quantification in SPECT. *Eur. J. Nucl. Med. Mol. Imaging* **38**(Suppl 1), S69–77 (2011).
15. Shcherbinin, S., Celler, A., Belhocine, T., Vanderwerf, R. & Driedger, A. Accuracy of quantitative reconstructions in SPECT/CT imaging. *Phys. Med. Biol.* **53**, 4595–4604 (2008).
16. Zeintl, J., Vija, A. H., Yahil, A., Hornegger, J. & Kuwert, T. Quantitative accuracy of clinical ^{99m}Tc SPECT/CT using ordered-subset expectation maximization with 3-dimensional resolution recovery, attenuation, and scatter correction. *J. Nucl. Med. Off. Publ. Soc. Nucl. Med.* **51**, 921–928 (2010).
17. Grudzinski, J. J. *et al.* Application of a whole-body pharmacokinetic model for targeted radionuclide therapy to NM404 and FLT. *Phys. Med. Biol.* **57**, 1641–1657 (2012).
18. Tian, M. *et al.* Whole-body biodistribution kinetics, metabolism, and radiation dosimetry estimates of 18F-PEG6-IPQA in nonhuman primates. *J. Nucl. Med. Off. Publ. Soc. Nucl. Med.* **52**, 934–941 (2011).
19. Nickel, M. *et al.* Development and evaluation of a pharmacokinetic model for prediction of radioimmunotherapy based on pretherapy data. *Cancer Biother. Radiopharm.* **24**, 111–122 (2009).
20. Fink-Bennett, D. M. & Thomas, K. ⁹⁰Y-ibritumomab tiuxetan in the treatment of relapsed or refractory B-cell non-Hodgkin's lymphoma. *J. Nucl. Med. Technol.* **31**, 61–68; quiz 69–70 (2003).

21. Ferrer, L. *et al.* Comparisons of dosimetric approaches for fractionated radioimmunotherapy of non-Hodgkin lymphoma. *Q. J. Nucl. Med. Mol. Imaging Off. Publ. Ital. Assoc. Nucl. Med. AIMN Int. Assoc. Radiopharmacol. IAR Sect. Soc. Of* **56**, 529–537 (2012).
22. McKeage, K. & Perry, C. M. Trastuzumab: a review of its use in the treatment of metastatic breast cancer overexpressing HER2. *Drugs* **62**, 209–243 (2002).
23. Gupta, A. K., Lad, V. J. & Koshy, A. A. Protection of mice against experimental Japanese encephalitis virus infections by neutralizing anti-glycoprotein E monoclonal antibodies. *Acta Virol.* **47**, 141–145 (2003).
24. Wiseman, G. A. *et al.* Biodistribution and dosimetry results from a phase III prospectively randomized controlled trial of Zevalin radioimmunotherapy for low-grade, follicular, or transformed B-cell non-Hodgkin's lymphoma. *Crit. Rev. Oncol. Hematol.* **39**, 181–194 (2001).
25. Villeneuve, J. *et al.* The hepatic microcirculation in the isolated perfused human liver. *Hepatology* **23**, 24–31 (1996).
26. Brambell, F. W., Hemmings, W. A. & Morris, I. G. A Theoretical Model of Gamma-Globulin Catabolism. *Nature* **203**, 1352–1354 (1964).
27. Junghans, R. P. & Waldmann, T. A. Metabolism of Tac (IL2Ralpha): physiology of cell surface shedding and renal catabolism, and suppression of catabolism by antibody binding. *J. Exp. Med.* **183**, 1587–1602 (1996).
28. Watanabe, T. *et al.* Phase I study of radioimmunotherapy with an anti-CD20 murine radioimmunoconjugate ((90)Y-ibritumomab tiuxetan) in relapsed or refractory indolent B-cell lymphoma. *Cancer Sci.* **96**, 903–910 (2005).
29. Meibohm, B. *Pharmacokinetics and Pharmacodynamics of Biotech Drugs: Principles and Case Studies in Drug Development.* (John Wiley & Sons, 2006).
30. Arrichiello, C. *et al.* Feasibility of bremsstrahlung dosimetry for direct dose estimation in patients undergoing treatment with ⁹⁰Y-ibritumomab tiuxetan. *Eur. J. Nucl. Med. Mol. Imaging* **39**, 956–966 (2012).
31. Conti, P. S. *et al.* The role of imaging with (111)In-ibritumomab tiuxetan in the ibritumomab tiuxetan (zevalin) regimen: results from a Zevalin Imaging Registry. *J. Nucl. Med. Off. Publ. Soc. Nucl. Med.* **46**, 1812–1818 (2005).
32. Fisher, D. R., Shen, S. & Meredith, R. F. MIRD dose estimate report No. 20: radiation absorbed-dose estimates for ¹¹¹In- and ⁹⁰Y-ibritumomab tiuxetan. *J. Nucl. Med. Off. Publ. Soc. Nucl. Med.* **50**, 644–652 (2009).
33. Minarik, D. *et al.* ⁹⁰Y Bremsstrahlung imaging for absorbed-dose assessment in high-dose radioimmunotherapy. *J. Nucl. Med. Off. Publ. Soc. Nucl. Med.* **51**, 1974–1978 (2010).
34. Cremonesi, M. *et al.* High-dose radioimmunotherapy with ⁹⁰Y-ibritumomab tiuxetan: comparative dosimetric study for tailored treatment. *J. Nucl. Med. Off. Publ. Soc. Nucl. Med.* **48**, 1871–1879 (2007).
35. Rizvi, S. N. F. *et al.* Biodistribution, radiation dosimetry and scouting of ⁹⁰Y-ibritumomab tiuxetan therapy in patients with relapsed B-cell non-Hodgkin's lymphoma using ⁸⁹Zr-ibritumomab tiuxetan and PET. *Eur. J. Nucl. Med. Mol. Imaging* **39**, 512–520 (2012).
36. Morschhauser, F. *et al.* ⁹⁰Yttrium-ibritumomab tiuxetan consolidation of first remission in advanced-stage follicular non-Hodgkin lymphoma: updated results after a median follow-up of 7.3 years from the International, Randomized, Phase III First-Line Indolent trial. *J. Clin. Oncol. Off. J. Am. Soc. Clin. Oncol.* **31**, 1977–1983 (2013).
37. Tout, M. *et al.* Rituximab exposure is influenced by baseline metabolic tumor volume and predicts outcome of DLBCL patients: a LYSA study. *Blood*, <https://doi.org/10.1182/blood-2016-10-744292> (2017).
38. Menke-van der Houven van Oordt, C. W. *et al.* ⁸⁹Zr-cetuximab PET imaging in patients with advanced colorectal cancer. *Oncotarget* **6**, 30384–30393 (2015).
39. Natarajan, A. & Gambhir, S. S. Radiation Dosimetry Study of [(89)Zr]rituximab Tracer for Clinical Translation of B cell NHL Imaging using Positron Emission Tomography. *Mol. Imaging Biol. MIB Off. Publ. Acad. Mol. Imaging* **17**, 539–547 (2015).
40. Singh, V. *et al.* Surface levels of CD20 determine anti-CD20 antibodies mediated cell death *in vitro*. *PLoS One* **9**, e111113 (2014).
41. Zettlitz, K. A. *et al.* ImmunoPET of Malignant and Normal B Cells with ⁸⁹Zr- and ¹²⁴I-Labeled Obinutuzumab Antibody Fragments Reveals Differential CD20 Internalization *In Vivo*. *Clin. Cancer Res.* **23**, 7242–7252 (2017).
42. Vaughan, A. T., Cragg, M. S. & Beers, S. A. Antibody modulation: Limiting the efficacy of therapeutic antibodies. *Pharmacol. Res.* **99**, 269–275 (2015).
43. Shen, S. *et al.* Improved prediction of myelotoxicity using a patient-specific imaging dose estimate for non-marrow-targeting (90)Y-antibody therapy. *J. Nucl. Med. Off. Publ. Soc. Nucl. Med.* **43**, 1245–1253 (2002).

Acknowledgements

The authors wish to thank the hospital staff who compiled the imaging data. The authors thank Mrs Alexandra Tavernier-Sommerville (M.A. (University of Glasgow, U.K), Professeur Agrégée (in English language), France) for the proofreading of the manuscript.

Author Contributions

Morschhauser F and Odou P designed the study. Morschhauser F, Dekyndt B, Décaudin B, Odou P wrote the manuscript. Morschhauser F, Dekyndt B, Baillet C, Barthélémy C, Malek E, Fulcrand J, Bigot P, Huglo D, Décaudin B, Simon N, Odou P contributed to the acquisition of study material, analysis, or interpretation of data for the work and approved the manuscript. All authors are accountable for all aspects of the work by ensuring that questions related to the accuracy or integrity of any part of the work are appropriately investigated and answered.

Additional Information

Competing Interests: The authors declare no competing interests.

Publisher's note: Springer Nature remains neutral with regard to jurisdictional claims in published maps and institutional affiliations.



Open Access This article is licensed under a Creative Commons Attribution 4.0 International License, which permits use, sharing, adaptation, distribution and reproduction in any medium or format, as long as you give appropriate credit to the original author(s) and the source, provide a link to the Creative Commons license, and indicate if changes were made. The images or other third party material in this article are included in the article's Creative Commons license, unless indicated otherwise in a credit line to the material. If material is not included in the article's Creative Commons license and your intended use is not permitted by statutory regulation or exceeds the permitted use, you will need to obtain permission directly from the copyright holder. To view a copy of this license, visit <http://creativecommons.org/licenses/by/4.0/>.

© The Author(s) 2018